

Signature of a doubly charm tetraquark pole in  $DD^*$  scattering on the latticeM. Padmanath<sup>1,2,\*</sup> and S. Prelovsek<sup>3,4,†</sup><sup>1</sup>*Helmholtz Institut Mainz, Mainz, Germany*<sup>2</sup>*GSI Helmholtzzentrum für Schwerionenforschung, Darmstadt, Germany*<sup>3</sup>*Faculty of Mathematics and Physics, University of Ljubljana, Ljubljana, Slovenia*<sup>4</sup>*Jozef Stefan Institute, Ljubljana, Slovenia*

The doubly charm tetraquark with flavor  $cc\bar{u}\bar{d}$  and isospin  $I = 0$  is investigated by calculating the  $DD^*$  scattering amplitude with lattice QCD. The simulation is done on CLS ensembles with dynamical  $u/d, s$  quarks and  $m_\pi \simeq 280$  MeV for two charm quark masses, one slightly larger and one slightly lower than the physical value. The scattering amplitudes for partial waves  $l = 0, 1$  are extracted near-threshold via the Lüscher's method by considering systems with total momenta  $PL/(2\pi) = 0, 1, \sqrt{2}, 2$  on two spatial volumes. A virtual bound state pole in the  $DD^*$  scattering amplitude with  $l = 0$  is found  $9.9^{+3.6}_{-7.1}$  MeV below  $DD^*$  threshold for the charm quark mass closer to the physical value. This pole is likely related to the doubly charm tetraquark discovered by LHCb less than 1 MeV below  $D^0D^{*+}$  threshold. Future lattice simulations closer to the continuum limit and physical quark masses would be valuable to establish this connection systematically.

*Introduction:* The LHCb collaboration recently discovered a doubly charmed tetraquark  $T_{cc}$  with flavor  $cc\bar{u}\bar{d}$  just  $0.36(4)$  MeV below  $D^0D^{*+}$  threshold [1, 2]<sup>1</sup>. Its flavor is based on the decay channel  $D^0D^0\pi^+$  and it has isospin  $I = 0$  since no state was found in the decay  $D^0D^+\pi^+$ . The total spin and parity  $J^P$  have not been determined from experiment. This is the longest-lived hadron discovered with explicitly exotic quark content. It has striking similarities with the well-known  $X(3872)$  [3] that lies very close to  $D^0\bar{D}^{*0}$  threshold. Here we aim at the theoretical investigation of near-threshold exotics from first principles.

Several phenomenological models predicted a doubly charm tetraquark  $cc\bar{u}\bar{d}$  with  $I = 0$  and  $J^P = 1^+$  within an energy range  $\pm 100$  MeV around the  $DD^*$  threshold, *e.g.* [4–12]. Many of these models have a possibility to identify a bound state but not a resonance. One of the more sophisticated quark model calculations predicted the bound state  $1.6 \pm 1.0$  MeV below  $DD^*$  threshold and concluded that the molecular Fock component dominates over the diquark antidiquark component [11]. Within a molecular picture, a light vector meson exchange is argued to induce attraction [13, 14], whereas one-pion exchange induces slight repulsion [15]. The binding energy of a bound state in the  $QQ\bar{u}\bar{d}$  system is found to decrease with decreasing heavy quark mass  $m_Q$  and with increasing light quark mass  $m_{u,d}$  [9, 11, 16–24]. Thus the doubly bottom tetraquarks  $bb\bar{u}\bar{d}$  and  $bb\bar{s}\bar{s}$  with  $J^P = 1^+$  are deeply bound according to variety of theoretical approaches [9, 11, 16–18, 20, 21, 23], whereas  $cc\bar{u}\bar{d}$  is expected on the verge of binding and requires a careful theoretical study within QCD.

In order to theoretically confirm the existence of a doubly charmed tetraquark from first-principles, one has to

establish a pole in the corresponding scattering amplitude  $t(E_{cm})$ . This is particularly important in finite-volume formulations, such as lattice QCD, since this state does not lie well below the threshold but is expected near threshold. Lattice QCD represents the only non-perturbative first-principles approach with quantifiable systematic and statistical uncertainties to study QCD in the hadronic regime. It enables the determination of the scattering amplitudes from deviations of finite-volume energies from the non-interacting scenario [25]. However, the scattering amplitude in this channel has not been determined using lattice simulations yet. The lattice study in Ref. [16] extracted the finite-volume energy of the ground state using meson-meson and diquark-antidiquark interpolators for a wide range of  $m_\pi \geq 260$  MeV and three lattice spacings. The continuum and chiral extrapolations lead to an energy level  $-23 \pm 11$  MeV relative to the  $DD^*$  threshold. This indicates the presence of interactions between  $D$  and  $D^*$ , but does not prove the existence of a pole. The finite-volume energies have been extracted in Ref. [26] and the ground state energy was found to be consistent with the  $DD^*$  threshold.

This letter investigates if a state with flavor  $cc\bar{u}\bar{d}$ ,  $I = 0$ , and  $J^P = 1^+$  exists in the vicinity of  $DD^*$  threshold. For this purpose,  $DD^*$  scattering amplitude  $t(E_{cm})$  near threshold is extracted within lattice QCD for the first time. It is determined from finite-volume energies via the Lüscher's method [25]. The  $D^*$  does not decay strongly to  $D\pi$  at the simulated  $m_\pi \simeq 280$  MeV and the analyzed energy region is below the  $DD\pi$  and  $D^*D^*$  thresholds, therefore we consider one-channel  $DD^*$  scattering. We demonstrate that the scattering amplitude indeed has a pole at  $E_{cm}^p$  slightly below threshold.

First we present the calculation of the energy levels. Then we discuss the extraction of the scattering amplitude and the poles in it.

*Ensembles and single-hadron masses:* We utilize two ensembles with  $u/d, s$  dynamical quarks provided by

\* pmadanag@uni-mainz.de, pappapan@gmail.com

† sasa.prelovsek@ijs.si

<sup>1</sup> The mass obtained from the pole position in Ref. [2] is quoted.

the Coordinated Lattice Simulations consortium [27, 28]. The lattice spacing is  $a = 0.08636(98)(40)$  fm,  $m_u$  and  $m_d$  are degenerate and heavier than in Nature, corresponding to  $m_\pi = 280(3)$  MeV. There are 255 configurations on spatial volume  $N_L^3 = 24^3$  and 492 configurations on  $32^3$  [29]. The scattering amplitude is extracted for two values of the charm quark mass, one slightly heavier than physical and one slightly lighter [30]. The masses of the relevant hadrons  $D$  and  $D^*$  are presented in Table II. The heavier charm quark mass is closer to the physical value and provides our main result.

*Interpolators and finite-volume energies:* In the non-interacting limit, the  $DD^*$  system has discrete energies on a periodic lattice of size  $L = N_L a$

$$E^{\text{ni}} = E_{D(\vec{p}_1)} + E_{D^*(\vec{p}_2)}, \quad \vec{p}_i = \vec{n}_i \frac{2\pi}{L}, \quad \vec{n}_i \in N_L^3 \quad (1)$$

with  $E_{H(\vec{p}_i)}^{\text{con}} = (m_H^2 + \vec{p}_i^2)^{1/2}$  in the continuum limit. The non-interacting energies are shown by lines in Fig. 1.

The finite-volume energies in the interacting theory are determined from the correlation matrices  $C_{ij}(t) = \langle O_i(t_{\text{src}} + t) O_j^\dagger(t_{\text{src}}) \rangle$ , where  $O_i$  refers to operators that annihilate states with the desired quantum numbers. The  $cc\bar{u}\bar{d}$  system is investigated in inertial frames with total momenta  $|\vec{P}|L/(2\pi) = 0, 1, \sqrt{2}, 2$  and finite-volume irreducible representations (irreps) in Table I. These constrain  $DD^*$  scattering in various partial waves  $l$ , of which  $l = 0$  is expected to dominate near threshold. We utilize only meson-meson interpolators, where each meson is projected to a definite momentum,

$$\begin{aligned} O^{DD^*} &= \sum_{k,j} A_{kj} D(\vec{p}_{1k}) D_j^*(\vec{p}_{2k}), \quad \vec{p}_{1k} + \vec{p}_{2k} = \vec{P} \quad (2) \\ &= \sum_{k,j} A_{kj} [(\bar{u}\Gamma_1 c)_{\vec{p}_{1k}} (\bar{d}\Gamma_2 j c)_{\vec{p}_{2k}} - (\bar{d}\Gamma_1 c)_{\vec{p}_{1k}} (\bar{u}\Gamma_2 j c)_{\vec{p}_{2k}}] \end{aligned}$$

with two choices  $(\Gamma_1, \Gamma_{2j}) = (\gamma_5, \gamma_j), (\gamma_5 \gamma_t, \gamma_j \gamma_t)$  throughout. Operators are shown in Section I of Ref. [31]. All quark fields are smeared according to the ‘Distillation’ method [30, 32] with 60(90) Laplacian eigenvectors for  $N_L = 24(32)$ .

The diquark-antidiquark interpolators  $[cc][\bar{d}\bar{u}]$  are not considered in this work. This is justified as it was observed in an earlier lattice calculation that such operators have negligible effects on the low-lying energies [26]. Indications from phenomenological studies on the dominance of molecular  $DD^*$  Fock components [11] also suggest that  $DD^*$  interpolators are sufficient to compute the energies faithfully. Furthermore, the application of two operators  $D_{\gamma_5} D_{\gamma_j}^*$  and  $D_{\gamma_5 \gamma_t} D_{\gamma_j \gamma_t}^*$  for each momentum combination is expected to provide enough variety to extract the energy levels reliably.

The energies  $E_n^{\text{lat}}$  are extracted from single-exponential fits to the eigenvalue correlators  $\lambda^{(n)}(t) \propto e^{-E_n^{\text{lat}} t}$  of the generalized eigenvalue problem  $C(t)v^{(n)}(t) = \lambda^{(n)}(t)C(t_0)v^{(n)}(t_0)$  with  $t_0 = 4$  [33]. In order to mitigate small deviations of single-hadron energies  $E_{H(\vec{p})}^{\text{lat}}$

from  $E_{H(\vec{p})}^{\text{con}}$  due to discretization effects, we take  $E_n = E_n^{\text{lat}} + E_{D(\vec{p}_1)}^{\text{con}} + E_{D^*(\vec{p}_2)}^{\text{con}} - E_{D(\vec{p}_1)}^{\text{lat}} - E_{D^*(\vec{p}_2)}^{\text{lat}}$  as the final energies for the scattering analysis, as argued and utilized on the same ensembles in Refs. [30, 34].

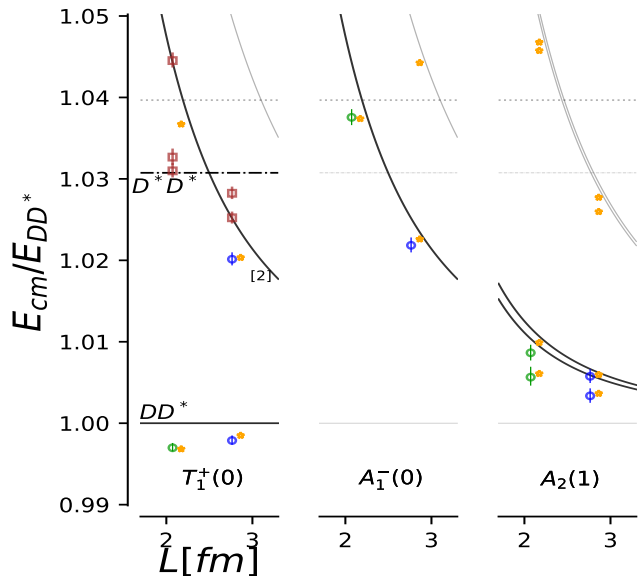


FIG. 1. The center-of-momentum energy  $E_{cm} = (E^2 - \vec{P}^2)^{1/2}$  of the  $cc\bar{u}\bar{d}$  system normalized by  $E_{DD^*} \equiv m_D + m_{D^*}$ , for the heavier charm quark mass in various finite-volume irreps. The lattice energy levels are shown by large circles and squares; the scattering analysis employs the blue and green circles. The non-interacting  $DD^*$  energies (1) are shown by lines: the operators related to black lines are employed, while those related to gray lines are omitted. Label [2] in  $T_1^+(0)$  refers to the multiplicity of non-interacting level  $D(1)D^*(1)$ . The orange stars represent the analytically reconstructed energy levels based on the fitted scattering amplitudes and are slightly horizontally shifted for clarity.

The resulting finite-volume energies in the first three irreps are presented in Fig. 1 for the heavier charm quark mass. The figure displays the energies  $E_{cm} = (E^2 - \vec{P}^2)^{1/2}$  in the center-of-momentum frame in units of energy of the  $DD^*$  threshold. The large circles and squares refer to the energy levels extracted from the lattice simulation. The energy levels have nonzero energy shifts with respect to the noninteracting  $DD^*$  energies indicating nontrivial interactions. These energy shifts render information on the  $DD^*$  scattering amplitudes. We find similar observations at the lighter charm quark mass [31].

*Scattering analysis:* The scattering amplitude  $t$  in  $S = e^{2i\delta} = 1 + i \frac{4\pi}{E_{cm}} t$  depends on energy, the partial wave  $l$  and  $J = |s - l|, \dots, |s + l|$ , where  $s = 1$  for  $DD^*$  system. We approximate their energy dependence near threshold

ID	$\vec{P}$	LG	$\Lambda^P$	$J^P$	$l$	interpolators: $M_1(\vec{p}_1^2)M_2(\vec{p}_2^2)$
1	(0, 0, 0)	$O_h$	$T_1^+$	$1^+$	0, 2	$D(0)D^*(0)$ , $D(1)D^*(1)$ [2], $D^*(0)D^*(0)$
2	(0, 0, 0)	$O_h$	$A_1^-$	$0^-$	1	$D(1)D^*(1)$
3	(0, 0, 1) $\frac{2\pi}{L}$	Dic <sub>4</sub>	$A_2$	$0^-, 1^+, 2^-$	0, 1, 2	$D(0)D^*(1)$ , $D(1)D^*(0)$
4	(1, 1, 0) $\frac{2\pi}{L}$	Dic <sub>2</sub>	$A_2$	$0^-, 1^+, 2^-, 2^+$	0, 1, 2	$D(0)D^*(2)$ , $D(1)D^*(1)$ [2], $D(2)D^*(0)$
5	(0, 0, 2) $\frac{2\pi}{L}$	Dic <sub>4</sub>	$A_2$	$0^-, 1^+, 2^-$	0, 1, 2	$D(1)D^*(1)$

TABLE I. Total momenta  $\vec{P}$ , spatial lattice symmetry group (LG), irreducible representations ( $\Lambda^P$ ) and interpolators considered for the system  $cc\bar{u}\bar{d}$ , together with total spin-parity  $J^P$  and partial-wave  $l$  of  $DD^*$  scattering that contributes to each irrep (only  $J, l \leq 2$  are listed). The interpolators are denoted by [2] when two linearly independent combinations of momenta and polarizations are employed, e.g.  $O_{l=0,2}$  for  $D(1)D^*(1)$  in  $T_1^+$  [31].

with two terms of the effective range expansion in  $p^2$  <sup>(2)</sup>

$$t_l^{(J)} = \frac{E_{cm}}{2} \frac{1}{p \cot \delta_l^{(J)} - ip}, \quad p^{2l+1} \cot \delta_l^{(J)} = \frac{1}{a_l^{(J)}} + \frac{r_l^{(J)}}{2} p^2, \quad (3)$$

where  $p = |\vec{p}|$  is the spatial-momentum of  $D$  and  $D^*$  in the center-of-momentum frame. Each finite-volume energy level  $E_{cm}$  is related to the  $t_l^{(J)}(E_{cm})$  via Lüscher's relation [25] and its generalizations, e.g. [35]. In order to constrain the energy dependence of  $t$ , the parameters of the effective range expansion are optimized such that Lüscher's relation is simultaneously satisfied for all the energy levels considered. For the  $l = 0$  partial wave, which dominates near threshold, we find

$$p \cot \delta_{l=0}^{(J=1)} = \frac{1}{a_0^{(1)}} + \frac{1}{2} r_0^{(1)} p^2 \quad (4)$$

$$m_c^{(h)} : a_0^{(1)} = 1.04(29) \text{ fm}, \quad r_0^{(1)} = 0.96({}_{-0.20}^{+0.18}) \text{ fm}.$$

This fit is shown by the red line in Fig. 2.

This result is robust to various fits we have performed, as further detailed in Ref. [31]. The  $J^P = 1^+$  is allowed for the  $DD^*$  system with spin one in partial waves  $l=0$  and  $l=2$ , which could lead to a partial wave mixing. We find that  $t_2^{(1)}$  is consistent with zero, since the energy levels with dominant overlaps to  $O_{l=2}$  [31] have energies consistent with the non-interacting energy (1). Hence we assume  $t_{l \geq 2}^{(J)} = 0$  and negligible mixing of  $l=2$  with  $l=0$  in  $J=1$  [31]. The energies in blue and green from Fig. 1 are utilized to constrain the energy dependence of  $t_0^{(1)}$  in Eq. (4) and  $t_1^{(0)}$ . We employ a combination of procedures outlined in Refs. [36, 37] in making our fits [31]. The fit has  $\chi^2/\text{dof} = 3.7/5$  and renders the parameters in Eq. (4) for  $l=0$  scattering and ( $a_1^{(0)} = 0.076({}_{-0.009}^{+0.008}) \text{ fm}^3$ ,  $r_1^{(0)} = 6.9(2.1) \text{ fm}^{-1}$ ) for  $l=1$  scattering. The fit results for  $t_1^{(0)}$  render poles significantly below threshold, at energies that are unconstrained by the energy levels, and therefore

we do not ascribe them any physical significance. The analytically reconstructed energies based on these  $t_l^J$  are indicated by orange stars in Fig. 1 and agree well with the observed energies.

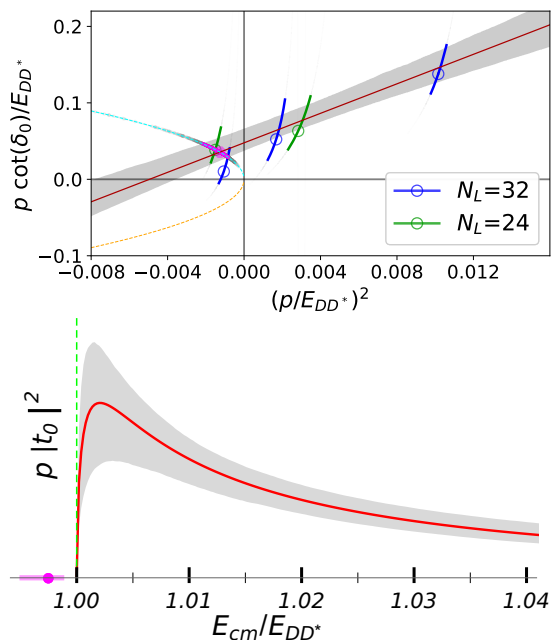


FIG. 2. Top:  $p \cot \delta_{l=0}^{(J=1)}$  for  $DD^*$  scattering at the heavier charm quark mass (red line) and  $ip = +|p|$  (cyan line) versus  $p^2$ , all normalized to  $E_{DD^*} \equiv m_D + m_{D^*}$ . The virtual bound state occurs at the momenta indicated by the magenta octagon, where two curves intersect. Bottom: The corresponding  $DD^*$  scattering rate  $N \propto p|t_0|^2$  above threshold along with the pole position.

*The pole in the  $DD^*$  scattering amplitude and  $T_{cc}$ :* Before focusing on  $T_{cc}$ , let us briefly review the relation between hadrons and poles. The existence a hadron state and its mass are inferred from the pole in the scattering amplitude  $t(E_{cm})$ . The bound state and the virtual bound state have pole at a real energy below threshold and therefore  $p^2 < 0$ . A bound state has pole at  $p = i|p_B|$  and is an asymptotic state, e.g. deuteron. A

<sup>2</sup> This relation omits mixing of partial waves for reasons discussed later, while the more general relation is provided in Ref. [31].

	$m_D$ [MeV]	$m_{D^*}$ [MeV]	$M_{av}$ [MeV]	$a_{l=0}^{(J=1)}$ [fm]	$r_{l=0}^{(J=1)}$ [fm]	$\delta m_{T_{cc}}$ [MeV]	$T_{cc}$
lat. ( $m_\pi \simeq 280$ MeV, $m_c^{(h)}$ )	1927(1)	2049(2)	3103(3)	1.04(29)	$0.96^{+0.18}_{-0.20}$	$-9.9^{+3.6}_{-7.2}$	virtual bound st.
lat. ( $m_\pi \simeq 280$ MeV, $m_c^{(l)}$ )	1762(1)	1898(2)	2820(3)	0.86(0.22)	$0.92^{+0.17}_{-0.19}$	$-15.0^{+4.6}_{-9.3}$	virtual bound st.
exp. [2, 38]	1864.85(5)	2010.26(5)	3068.6(1)	-7.15(51)	$[-11.9(16.9), 0]$	-0.36(4)	bound st.

TABLE II. Lattice results for the binding energy  $\delta m_{T_{cc}}$  and the effective range parameters in Eq. (3) at heavier ( $m_c^{(h)}$ ) and lighter ( $m_c^{(l)}$ ) charm quark masses, compared to experiment.  $m_c^{(h)}$  is closer to the physical value according to the spin averaged charmonium mass  $M_{av} \equiv \frac{1}{4}(m_{\eta_c} + 3m_{J/\psi})$ . The real part of experimental  $a_0^{(1)}$  is provided. The binding energy  $\delta m_{T_{cc}} \equiv \text{Re}(E_{cm}^p) - m_{D^0} - m_{D^{*+}}$  is obtained from the energy  $E_{cm}^p$ , where the scattering amplitude has a pole. Lattice results are shown with  $1\sigma$  statistical errors at given quark masses and lattice spacing; the  $T_{cc}$  is found to be a virtual bound state with  $\delta m_{T_{cc}} < 0$  also within  $2\sigma$  and  $3\sigma$  error ranges.

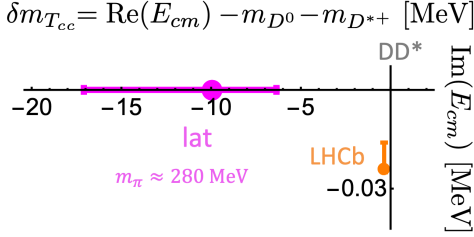


FIG. 3. The pole in the scattering amplitude related to  $T_{cc}$  in the complex energy plane: our lattice result at the heavier charm quark mass (magenta) and the LHCb result (orange).

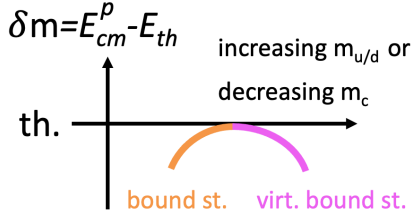


FIG. 4. Sketch of the binding energy for the (virtual) bound state dominated by the molecular component. It is based on a purely attractive potential  $V(r)$  and partial wave  $l = 0$  within quantum mechanics.

virtual bound state has a pole at  $p = -i|p_B|$  and is less familiar, it appears for example in  $^1S_0$  nucleon-nucleon channel [31, 39, 40]. Finally, the most common poles with  $E_{cm}$  away from the real axis correspond to decaying resonances, e.g.  $\rho$  meson.

We find a virtual bound state pole in  $DD^*$  scattering amplitude  $t_{l=0}^{(J=1)}$  at energy  $E_{cm}^p = (m_D^2 - |p_B|^2)^{1/2} + (m_{D^*}^2 - |p_B|^2)^{1/2}$ . It corresponds to the binding momentum indicated by the magenta octagon in Fig. 2. We therefore find an evidence for the doubly charmed tetraquark as a virtual bound state with binding energy

$$m_c^{(h)} : \delta m_{T_{cc}} = E_{cm}^p - m_D - m_{D^*} = -9.9^{+3.6}_{-7.1} \text{ MeV}. \quad (5)$$

It is situated slightly below  $DD^*$  threshold, close to the mass of the doubly charmed tetraquark  $T_{cc}$  discovered by

LHCb [1, 2]. The state found on the lattice is strongly stable and the pole appears at real energy since  $D^* \rightarrow D\pi$  is not kinematically allowed for  $m_\pi \simeq 280$  MeV. The  $T_{cc}$  discovered by LHCb decays to  $D^0 D^0 \pi^+$  and the pole is slightly imaginary, as shown in Fig. 3. The  $T_{cc}$  found in experiment would be a bound state in the limit of stable  $D^{*+}$  since the measured  $a_0^{(1)}$  is negative [2].

The quark mass dependence of  $T_{cc}$  and the notion of a virtual bound state can be most easily illustrated for s-wave scattering in purely attractive potential  $V(r)$  within quantum mechanics. Explicit toy-model examples are given in Refs. [31, 41]. The bound state occurs at  $p = i|p_B|$ , its wave function falls as  $e^{ipr} = e^{-|p_B|r}$  outside the potential and is an asymptotic state. As the potential depth is weakened, the bound state energy approaches threshold. As the potential is weakened even further so that it is not attractive enough to form a bound state, the s-wave bound state typically becomes a virtual bound state. It occurs at  $p = -i|p_B|$  and its wave function  $e^{ipr} = e^{|p_B|r}$  outside  $V$  is not normalizable, therefore it is not an asymptotic state. Even so, it gives rise to an abrupt enhancement in the scattering cross-section above the threshold when the pole is close below threshold. This enhancement is shown in Fig. 2 for  $DD^*$  scattering and appears due to virtual bound state  $T_{cc}$  in our study.

We expect that the virtual bound state pole found in our lattice simulation at unphysical  $u/d$  masses is related to the  $T_{cc}$  discovered by LHCb, as detailed in Section IV of [31]. The would-be LHCb bound state is expected to become a virtual bound state with increasing  $m_{u/d}$ . This is sketched in Fig. 4 for a tetraquark with a significant molecular  $DD^*$  component attracted by the Yukawa-like potential  $V(r) \propto e^{-Mr}/r$ , where the mass of the exchanged light hadron  $M$  increases with increasing  $m_{u/d}$ .

A near-threshold virtual bound state pole is also observed for the lighter charm quark mass with a slightly larger  $|\delta m_{T_{cc}}|$ , as listed in Table II. This observation is consistent with the dependence of pole position on  $m_c$  sketched in Fig. 4. This arises within quantum mechanics via the reduced  $DD^*$  mass for purely attractive po-

tential  $V(r)$  that is assumed to be flavor blind<sup>3</sup>.

*Conclusions:* We have performed a simulation of  $DD^*$  scattering in lattice QCD at  $m_\pi \simeq 280$  MeV. Unlike other existing lattice investigations in this regard, we extracted the near-threshold scattering amplitudes in the flavor channel  $cc\bar{u}\bar{d}$  with isospin  $I = 0$ . Scattering amplitudes for partial waves  $l=0, 1$  are determined via the Lüscher's method, and a virtual bound state pole is found for the partial wave  $l=0$ . The doubly charm tetraquark with  $J^P = 1^+$  features as a virtual bound state  $9.9_{-7.1}^{+3.6}$  MeV below threshold in our simulation with charm quark mass slightly larger than physical. We also observe that the size of the binding energy for this virtual bound state increases with decreasing charm quark mass.

*Outlook:* Future lattice studies are desired to reaffirm our findings and inferences. The current knowledge could be improved by adding diquark-antidiquark interpolators, exploring dependence on quark masses and investigation of discretization effects based on improved actions and at smaller lattice spacings. The simulations at smaller  $m_{u/d}$  are required to establish whether the pole will approach the  $DD^*$  threshold. The simulations at physical  $m_{u/d}$  will be challenging due to the strong de-

cays  $D^* \rightarrow D\pi$  and  $T_{cc} \rightarrow DD\pi$ , while the formalism is already available in [43].

## ACKNOWLEDGMENTS

We would particularly like to thank Sara Collins and the members of the RQCD for discussions and support related to the computer resources used in this project. We are grateful to J. J. Dudek, J. R. Green, F.-K. Guo, A. D. Hanlon, B. Hörz, M. Karliner, L. Leskovec, M. Mai, N. Mathur, D. Mohler, E. Oset, S. Paul, M. Rosina, M. Sadl, S. Sharpe, and B.-S. Zou for valuable discussions. We thank our colleagues in CLS for the joint effort in the generation of the gauge field ensembles which form a basis for the computation. The correlators were computed on the Regensburg Athene2 cluster. We thank the authors of Ref. [36] for making the *TwoHadronsInBox* package public and C. B. Lang for contributions to the computing codes we used. S. P. acknowledges support by Slovenian Research Agency ARRS (research core funding No. P1-0035).

- 
- [1] LHCb, R. Aaij *et al.*, 2109.01038.  
 [2] LHCb, R. Aaij *et al.*, 2109.01056.  
 [3] Belle, S. K. Choi *et al.*, Phys. Rev. Lett. **91**, 262001 (2003), [arXiv:hep-ex/0309032].  
 [4] J. P. Ader, J. M. Richard and P. Taxil, Phys. Rev. D **25**, 2370 (1982).  
 [5] L. Heller and J. A. Tjon, Phys. Rev. D **35**, 969 (1987).  
 [6] J. Carlson, L. Heller and J. A. Tjon, Phys. Rev. D **37**, 744 (1988).  
 [7] F. S. Navarra, M. Nielsen and S. H. Lee, Phys. Lett. B **649**, 166 (2007), [arXiv:hep-ph/0703071].  
 [8] D. Ebert, R. N. Faustov, V. O. Galkin and W. Lucha, Phys. Rev. D **76**, 114015 (2007), [arXiv:0706.3853].  
 [9] M. Karliner and J. L. Rosner, Phys. Rev. Lett. **119**, 202001 (2017), [arXiv:1707.07666].  
 [10] E. J. Eichten and C. Quigg, Phys. Rev. Lett. **119**, 202002 (2017), [arXiv:1707.09575].  
 [11] D. Janc and M. Rosina, Few Body Syst. **35**, 175 (2004), [arXiv:hep-ph/0405208].  
 [12] T. F. Carames, A. Valcarce and J. Vijande, Phys. Lett. B **699**, 291 (2011).  
 [13] A. Feijoo, W. H. Liang and E. Oset, Phys. Rev. D **104**, 114015 (2021), [arXiv:2108.02730].  
 [14] X.-K. Dong, F.-K. Guo and B.-S. Zou, Commun. Theor. Phys. **73**, 125201 (2021), [arXiv:2108.02673].  
 [15] M.-L. Du *et al.*, Phys. Rev. D **105**, 014024 (2022), [arXiv:2110.13765].  
 [16] P. Junnarkar, N. Mathur and M. Padmanath, Phys. Rev. D **99**, 034507 (2019), [arXiv:1810.12285].  
 [17] M. Pflaumer, L. Leskovec, S. Meinel and M. Wagner, Existence and Non-Existence of Doubly Heavy Tetraquark Bound States, in *38th International Symposium on Lattice Field Theory*, 2021, [2108.10704].  
 [18] A. Francis, R. J. Hudspith, R. Lewis and K. Maltman, Phys. Rev. Lett. **118**, 142001 (2017), [arXiv:1607.05214].  
 [19] A. Francis, R. J. Hudspith, R. Lewis and K. Maltman, Phys. Rev. D **99**, 054505 (2019), [arXiv:1810.10550].  
 [20] L. Leskovec, S. Meinel, M. Pflaumer and M. Wagner, Phys. Rev. D **100**, 014503 (2019), [arXiv:1904.04197].  
 [21] B. Colquhoun, A. Francis, R. J. Hudspith, R. Lewis and K. Maltman, , in *38th International Symposium on Lattice Field Theory*, 2022.  
 [22] R. J. Hudspith, B. Colquhoun, A. Francis, R. Lewis and K. Maltman, Phys. Rev. D **102**, 114506 (2020), [arXiv:2006.14294].  
 [23] P. Bicudo, K. Cichy, A. Peters, B. Wagenbach and M. Wagner, Phys. Rev. D **92**, 014507 (2015), [arXiv:1505.00613].  
 [24] A. Francis, P. de Forcrand, R. Lewis and K. Maltman, 2106.09080.  
 [25] M. Luscher, Nucl. Phys. B **354**, 531 (1991).  
 [26] Hadron Spectrum, G. K. C. Cheung, C. E. Thomas, J. J. Dudek and R. G. Edwards, JHEP **11**, 033 (2017), [arXiv:1709.01417].  
 [27] M. Bruno *et al.*, JHEP **02**, 043 (2015), [arXiv:1411.3982].  
 [28] RQCD, G. S. Bali, E. E. Scholz, J. Simeth and W. Söldner, Phys. Rev. **D94**, 074501 (2016), [arXiv:1606.09039].  
 [29] M. Bruno, T. Korzec and S. Schaefer, Phys. Rev. **D95**, 074504 (2017), [arXiv:1608.08900].  
 [30] S. Piemonte, S. Collins, D. Mohler, M. Padmanath

<sup>3</sup> Or else, the lattice results for the binding energy at various heavy quark masses can be used to examine how good is the heavy flavor symmetry in line with Ref. [42].

- and S. Prelovsek, Phys. Rev. D **100**, 074505 (2019), [arXiv:1905.03506].
- [31] *See the supplemental material for the details of the operators utilized, the fitting procedure, the results from amplitude fits and discussion on heavy quark mass dependence of the near-threshold state. This includes Refs. [9, 11, 16–21, 23, 24, 34–37, 39–41, 44].*
- [32] Hadron Spectrum, M. Peardon *et al.*, Phys. Rev. D **80**, 054506 (2009), [arXiv:0905.2160].
- [33] C. Michael, Nucl. Phys. B **259**, 58 (1985).
- [34] S. Prelovsek, S. Collins, D. Mohler, M. Padmanath and S. Piemonte, JHEP **06**, 035 (2021), [arXiv:2011.02542].
- [35] R. A. Briceño, Phys. Rev. D **89**, 074507 (2014), [arXiv:1401.3312].
- [36] C. Morningstar *et al.*, Nucl. Phys. B **924**, 477 (2017), [arXiv:1707.05817].
- [37] Hadron Spectrum, A. J. Woss, D. J. Wilson and J. J. Dudek, Phys. Rev. D **101**, 114505 (2020), [arXiv:2001.08474].
- [38] Particle Data Group, P. Zyla *et al.*, PTEP **2020**, 083C01 (2020).
- [39] I. Matuschek, V. Baru, F.-K. Guo and C. Hanhart, Eur. Phys. J. A **57**, 101 (2021), [arXiv:2007.05329].
- [40] P. Reinert, H. Krebs and E. Epelbaum, Eur. Phys. J. A **54**, 86 (2018), [arXiv:1711.08821].
- [41] *See the supplemental material video file. Demonstration of trajectory of the pole singularity in an attractive Gaussian potential  $V = -V_0 e^{-r^2/R^2}$ .*
- [42] V. Baru *et al.*, Eur. Phys. J. C **79**, 46 (2019), [arXiv:1810.06921].
- [43] T. D. Blanton and S. R. Sharpe, Phys. Rev. D **104**, 034509 (2021), [arXiv:2105.12094].
- [44] S. Prelovsek, U. Skerbis and C. B. Lang, JHEP **01**, 129 (2017), [arXiv:1607.06738].

## Supplemental material

This supplemental material provides further information on our study of the doubly charm tetraquark channel. We present the interpolators relevant for the scattering of a pseudoscalar particle and a vector particle, effective energies and the details on how the scattering amplitudes are extracted. The notion of the virtual bound state is illustrated in quantum mechanics. The dependence of  $T_{cc}$  pole on the quark masses is investigated based on simple quantum mechanical arguments.

### I. INTERPOLATORS

This section presents the explicit expressions for two-meson interpolators that transform according to the irreducible representations  $\Lambda$  in Table 1 of the main article. They are relevant for the scattering of a pseudoscalar meson  $P$  and a vector meson  $V$ , so they are valuable for  $DD^*$  scattering simulated in this work and also for many interesting channels like  $BB^*$ ,  $\pi J/\psi$ ,  $KD^*$  etc. Each meson is projected to a definite momentum, which is given in units of  $2\pi/L$  in parenthesis. The linear combinations of momenta and vector-meson polarizations are chosen such that the operators transform according to the finite-volume irreps. They are obtained with the partial-wave method for total momentum  $\vec{P} = \vec{0}$  [44]. For  $\vec{P} \neq \vec{0}$  we consider only the one-dimensional irreducible representations and the operators are obtained with the projection method as  $O = \sum_{R \in LG} \chi^\Lambda(R) R P(\vec{p}_1) V_k(\vec{p}_2) R^{-1}$ , where  $\chi^\Lambda(R)$  is the character. The operators indicated by  $O$  were analyzed in the present simulation, while operators indicated by  $O'$  were not implemented and may be valuable for future studies:

$$T_1^+, \vec{P} = \{0, 0, 0\}, \text{ row } z$$

$$O^{l=0} = P(\{0, 0, 0\})V_z(\{0, 0, 0\})$$

$$O^{l=0} = P(\{1, 0, 0\})V_z(\{-1, 0, 0\}) + P(\{-1, 0, 0\})V_z(\{1, 0, 0\}) \\ + P(\{0, 1, 0\})V_z(\{0, -1, 0\}) + P(\{0, -1, 0\})V_z(\{0, 1, 0\}) \\ + P(\{0, 0, 1\})V_z(\{0, 0, -1\}) + P(\{0, 0, -1\})V_z(\{0, 0, 1\})]$$

$$O^{l=2} = P(\{1, 0, 0\})V_z(\{-1, 0, 0\}) + P(\{-1, 0, 0\})V_z(\{1, 0, 0\}) \\ + P(\{0, 1, 0\})V_z(\{0, -1, 0\}) + P(\{0, -1, 0\})V_z(\{0, 1, 0\}) \\ - 2[P(\{0, 0, 1\})V_z(\{0, 0, -1\}) + P(\{0, 0, -1\})V_z(\{0, 0, 1\})]$$

$$O^{l=0} = V_{1x}[0, 0, 0]V_{2y}[0, 0, 0] - V_{1y}[0, 0, 0]V_{2x}[0, 0, 0]$$

$$A_1^-, \vec{P} = \{0, 0, 0\}$$

$$O = P(\{1, 0, 0\})V_x(\{-1, 0, 0\}) - P(\{-1, 0, 0\})V_x(\{1, 0, 0\}) \\ + P(\{0, 1, 0\})V_y(\{0, -1, 0\}) - P(\{0, -1, 0\})V_y(\{0, 1, 0\}) \\ + P(\{0, 0, 1\})V_z(\{0, 0, -1\}) - P(\{0, 0, -1\})V_z(\{0, 0, 1\})$$

$$A_2, \vec{P} = \{0, 0, 1\}$$

$$O = P(\{0, 0, 0\})V_z(\{0, 0, 1\})$$

$$O = P(\{0, 0, 1\})V_z(\{0, 0, 0\})$$

$$O' = P(\{1, 0, 1\})V_x(\{-1, 0, 0\}) - P(\{-1, 0, 1\})V_x(\{1, 0, 0\}) \\ + P(\{0, 1, 1\})V_y(\{0, -1, 0\}) - P(\{0, -1, 1\})V_y(\{0, 1, 0\})$$

$$O' = P(\{1, 0, 1\})V_z(\{-1, 0, 0\}) + P(\{-1, 0, 1\})V_z(\{1, 0, 0\}) \\ + P(\{0, 1, 1\})V_z(\{0, -1, 0\}) + P(\{0, -1, 1\})V_z(\{0, 1, 0\})$$

$$O' = P(\{1, 0, 0\})V_x(\{-1, 0, 1\}) - P(\{-1, 0, 0\})V_x(\{1, 0, 1\}) \\ + P(\{0, 1, 0\})V_y(\{0, -1, 1\}) - P(\{0, -1, 0\})V_y(\{0, 1, 1\})$$

$$O' = P(\{1, 0, 0\})V_z(\{-1, 0, 1\}) + P(\{-1, 0, 0\})V_z(\{1, 0, 1\}) \\ + P(\{0, 1, 0\})V_z(\{0, -1, 1\}) + P(\{0, -1, 0\})V_z(\{0, 1, 1\})$$

$$A_2, \vec{P} = \{1, 1, 0\}$$

$$O = P(\{0, 0, 0\})(V_x(\{1, 1, 0\}) + V_y(\{1, 1, 0\}))$$

$$O = P(\{1, 0, 0\})V_x(\{0, 1, 0\}) + P(\{0, 1, 0\})V_y(\{1, 0, 0\})$$

$$O = P(\{0, 1, 0\})V_x(\{1, 0, 0\}) + P(\{1, 0, 0\})V_y(\{0, 1, 0\})$$

$$O = P(\{1, 1, 0\})(V_x(\{0, 0, 0\}) + V_y(\{0, 0, 0\}))$$

$$A_2, \vec{P} = \{0, 0, 2\}$$

$$O = P(\{0, 0, 1\})V_z(\{0, 0, 1\})$$

$$O' = P(\{0, 0, 0\})V_z(\{0, 0, 2\})$$

$$O' = P(\{0, 0, 2\})V_z(\{0, 0, 0\})$$

The number of pseudoscalar-vector eigen-states is equal to the number of interpolators in the non-interacting limit. This renders degenerate eigenstates in non-interacting limit that are indicated by [2] in Fig. 1 of the main article. This is responsible for nearly degenerate states in interacting theory - we observe all the expected nearly degenerate states in our finite volume energy levels. The current study also employs the  $D^*D^*$  interpolator for the  $T_1^+$  irrep and considers the levels below  $D^*D^*$  threshold in the scattering analysis.

## II. FINITE-VOLUME ENERGIES AND EFFECTIVE ENERGIES

Examples of effective energies are shown in Fig. 1 for the irreducible representation  $T_1^+$  and  $N_L = 32$ . Energy estimates from single exponential fits in the plateaued regions are indicated by red horizontal lines. The resulting finite-volume energies for all five irreducible representations and both volumes  $N_L = 24, 32$  are shown in Figs. 2 and 3 for two charm quark masses, respectively.

These results are obtained from the correlation matrices that are averaged over all spin and momentum polarizations and over several source timeslices  $t_{src}$ .

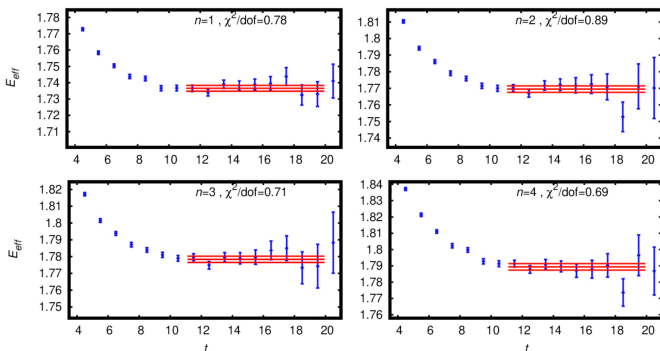


FIG. 1. Effective energies  $E_{\text{eff}}$  for irreducible representation  $T_1^+$  and  $N_L = 32$ .

## III. DETAILS OF SCATTERING ANALYSIS

In this section, we discuss the details of our procedure for extracting the scattering amplitude  $t$  in Eq. (4) from the finite-volume energies and present a summary of various fits we have performed. The best fit values of parameters in the effective range expansion describing the energy dependence of  $t$  are determined by minimizing a  $\chi^2$  function defined as

$$\chi^2(\{a\}) = \sum_L \sum_{\vec{P}\Lambda n} \sum_{\vec{P}'\Lambda'n'} dE_{cm}(L, \vec{P}\Lambda n; \{a\}) C^{-1}(L; \vec{P}\Lambda n; \vec{P}'\Lambda'n') dE_{cm}(L, \vec{P}'\Lambda'n'; \{a\}). \quad (1)$$

Here

$$dE_{cm}(L, \vec{P}\Lambda n; \{a\}) = E_{cm}(L, \vec{P}\Lambda n) - E_{cm}^{an.}(L, \vec{P}\Lambda n; \{a\})$$

is the difference between an observed lattice energy level  $E_{cm}(L, \vec{P}\Lambda n)$  and the analytically calculated energy level  $E_{cm}^{an.}(L, \vec{P}\Lambda n; \{a\})$  that satisfies the generalized Lüscher's equation [35, 36]

$$\det[(\tilde{K}_{ls;l's'}^{(J)}(E_{cm}, \{a\}))^{-1} \delta_{JJ'} - \delta_{ss'} B_{lJ;l'J'}^{\vec{P}, \Lambda}(E_{cm})] = 0 \quad (2)$$

for a given set of parameter values  $\{a\}$ . The  $B$  is a known kinematical matrix, computed using the *TwoHadronsInBox* package [36] and  $\tilde{K}^{-1}(E_{cm}, \{a\})$  is related to  $t$  as

$$(t_{ls;l's'}^{(J)})^{-1} = \frac{2(\tilde{K}_{ls;l's'}^{(J)}(E_{cm}, \{a\}))^{-1}}{E_{cm} p^l p^{l'}} - i \frac{2p \delta_{ll'} \delta_{ss'}}{E_{cm}}. \quad (3)$$

Here  $(l, s, J)$  refer to the partial-wave, the total spin and the total angular momentum of the incoming particles involved in the scattering, whereas the primed variables refer to that of the outgoing particles. The data covariance  $\mathcal{C}(L; \vec{P}\Lambda n; \vec{P}'\Lambda'n')$  is determined using the procedure outlined in Appendix A of Ref. [34]. The solutions of the Lüscher's equation (2) are extracted from the zeros in eigenvalues (as a function of  $E_{cm}$  for each lattice QCD ensemble and finite-volume irrep) of the matrix

$$\tilde{A}(E_{cm}) = \frac{A}{\det((\mu^2 + AA^\dagger)^{1/2})}, \quad (4)$$

by performing an eigenvalue decomposition along the lines as discussed in Ref. [37]. Here  $A$  is the argument of determinant in Eqn. 2 and  $\mu = 2.0$  is chosen throughout the calculation. We find our results are independent of the value of  $\mu$  across a wide interval  $[0.1, 100]$ .

Under the assumption that any contribution from  $l \geq 2$  partial waves are negligible<sup>4</sup>,  $\tilde{K}^{-1}(E_{cm}, \{a\})$  for elastic  $DD^*$  scattering reduces to a  $3 \times 3$  diagonal matrix, where elements are related to  $t$  and  $\delta$  as follows

$$(t_l^{(J)})^{-1} = \frac{2(\tilde{K}_l^{(J)})^{-1}}{E_{cm} p^{2l}} - i \frac{2p}{E_{cm}}, \quad (\tilde{K}_l^{(J)})^{-1} = p^{2l+1} \cot \delta_l^{(J)} \quad (5)$$

We parametrize it with the effective range expansion

$$\tilde{K}^{-1} = \begin{bmatrix} \frac{1}{a_0^{(1)}} + \frac{r_0^{(1)} p^2}{2} & 0 & 0 \\ 0 & \frac{1}{a_1^{(0)}} + \frac{r_1^{(0)} p^2}{2} & 0 \\ 0 & 0 & \frac{1}{a_1^{(2)}} \end{bmatrix}. \quad (6)$$

We perform separate and combined fits to the  $J^P(l) = 1^+(0), 0^-(1)$  channels (first two rows in the above  $\tilde{K}^{-1}$  matrix) using  $T_1^+$  and  $A_1^-$  irreps in the rest frame and  $A_2$  irrep in the moving frame with  $\vec{P} = (0, 0, 1) \frac{2\pi}{L}$ . Possible effects from the left-hand cuts are omitted. The fitting details, quality, results, and the parameter covariance for all fits in the two  $m_c$  we studied are listed in Table I. It is evident that the best fit parameters for  $l = 0$   $DD^*$

<sup>4</sup> All the energy levels with dominant overlap to operators with  $l = 2$  partial waves are consistent with the respective non-interacting energies. Any contribution of  $l \geq 2$  partial waves on the finite volume levels close to the  $DD^*$  threshold, which is the energy region of interest, are suppressed by the phase space factor  $p^{2l}$ . The extraction of any other effects from  $l \geq 2$  partial waves need the utilization of larger volume ensembles, which is beyond the scope of this work.



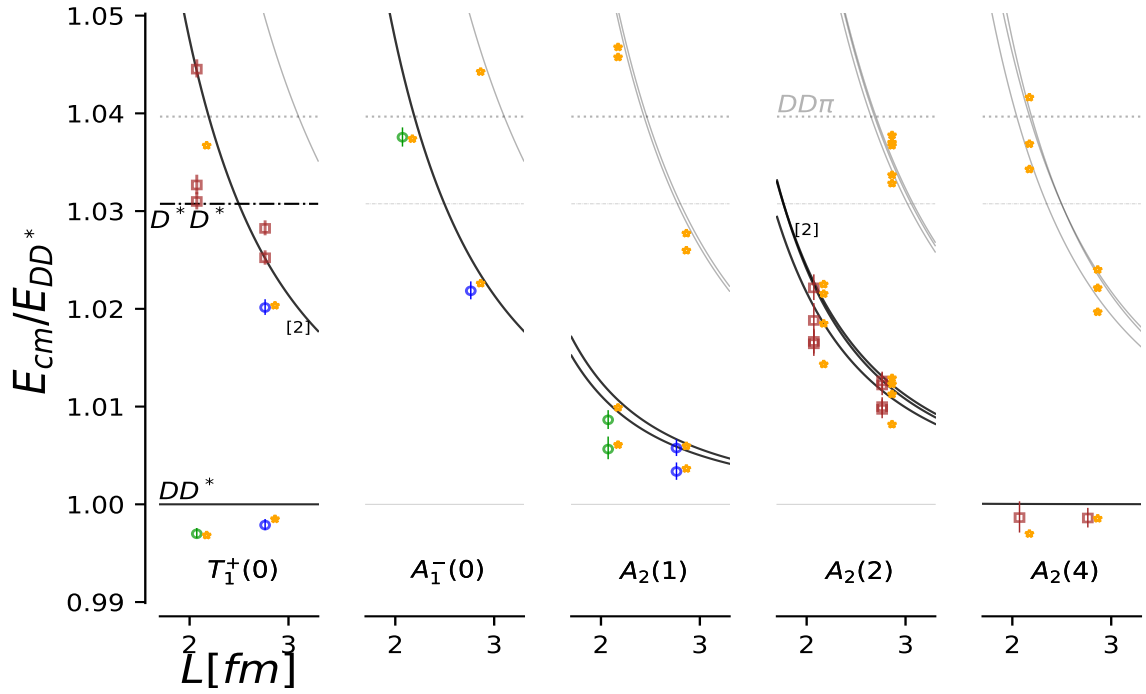


FIG. 2. Finite-volume energy levels ( $E_{cm}$ ) in the center-of-momentum frame in units of  $E_{DD^*} \equiv m_D + m_{D^*}$  for the heavier charm quark mass  $m_c^{(h)}$ . The results from lattice simulation are shown by empty circles and squares: blue and green circles are employed in the extraction of  $DD^*$  scattering amplitude with  $l = 0, 1$ . The non-interacting  $DD^*$  energies (Eq. (1) in the main text) are shown by lines: the operators related to black lines are considered, while the those related to the gray lines are omitted from the calculation. [2] in  $T_1^+(0)$  and  $A_2(2)$  refers to the multiplicity of non-interacting level  $D(1)D^*(1)$ , in these irreps. The orange stars represent the analytically predicted energies based on the fitted scattering amplitudes and are slightly horizontally shifted for clarity.

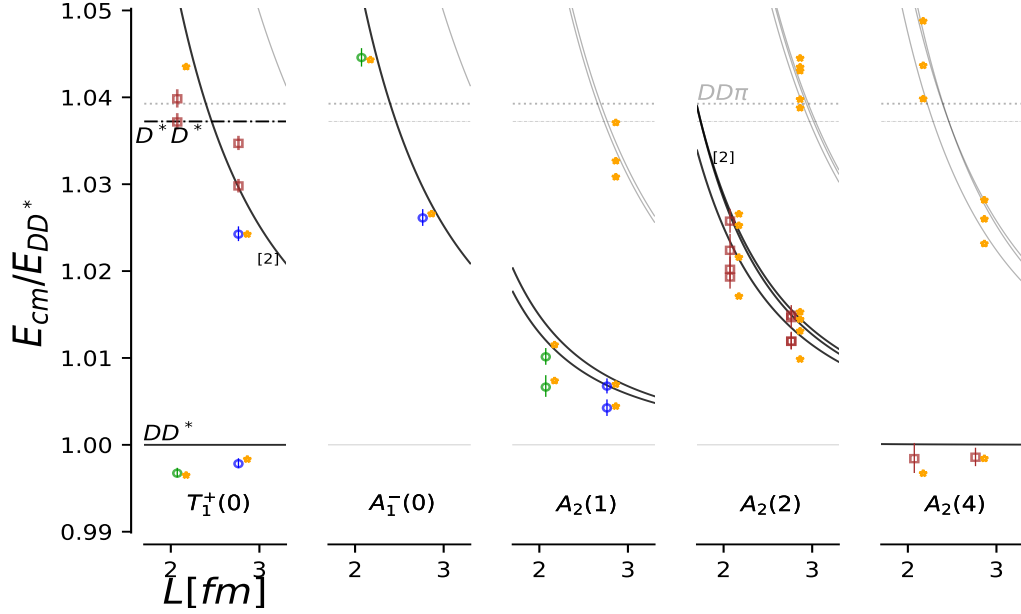


FIG. 3. Same as in Fig. 2, but for the lighter charm quark mass  $m_c^{(l)}$ .

scattering amplitude is stable with respect to separate and combined fits in the low energy region.  $p \cot(\delta_0)$  as

a function of  $p^2$  is presented in Fig. 2 of the main text and Fig. 4 below for the  $m_c^{(h)}$  and  $m_c^{(l)}$ , respectively.

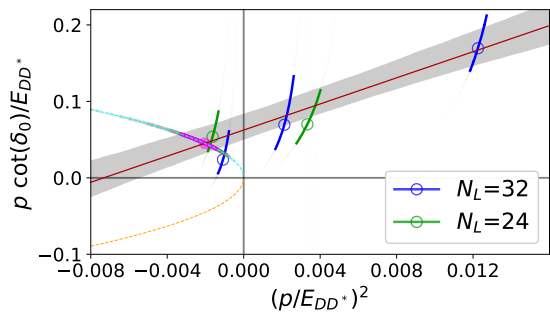


FIG. 4.  $p \cot \delta_{l=0}^{(J=1)}$  versus  $p^2$  in units of  $E_{DD^*} \equiv m_D + m_{D^*}$  for  $DD^*$  scattering at the light charm quark mass. The (cyan) orange dashed curve refers to the (virtual) bound state constraint. Green and blue circles indicate the simulated data, whereas the solid red curve along with the gray band are the fit results. The virtual bound state occurs at the momenta indicated by the magenta octagon, where red and cyan curves intersect.

In order to affirm our findings, we analytically predict the finite-volume energies in all five irreps. For this, we assume the full form of the  $\tilde{K}^{-1}$  matrix in Eq. (6) taking fit results with ID (2) and (4) in Table I and a small constant value for  $a_1^{(2)}$  to imitate a non-interacting scenario in this channel. This is then compared with the simulated finite volume energies to assess the quality of prediction. The  $\chi^2/dof$  evaluated using the predicted energies and the simulated results are 23/14 and 30/14 for the  $m_c^{(h)}$  and  $m_c^{(l)}$ , and are presented in Figs. 2 and 3, respectively. We find that the pattern of predicted and simulated finite volume energies are consistent, as shown by the smaller and larger symbols in these figures. We also observe that expanding the  $\tilde{K}^{-1}$  matrix to include nearly non-interacting  $J^P(l) = 1^+(2), 2^+(2)$  channels, also involving a possible mild partial wave mixing between  $J^P(l) = 1^+(0)$  and  $J^P(l) = 1^+(2)$  does not alter the finite-volume energies up to  $E_{cm}/E_{DD^*} = 1.025$  and also leads to the same  $\chi^2/dof$  value. In short, we find that our estimate for  $DD^*$  scattering amplitude with  $l = 0$  is robust to contaminations from other possible nearby channels.

#### IV. BOUND STATES, VIRTUAL BOUND STATES AND THEIR DEPENDENCE ON QUARK MASSES

Here we provide a simple quantum mechanical illustration of a virtual bound state and a more familiar bound state. Then we argue that one state can convert to the other as the quark masses change, and we explore their binding energies. The aim is to argue that the  $T_{cc}$  pole determined from lattice simulation and from the experiment roughly varies with changing  $m_{u/d}$  or  $m_c$

as sketched in Fig. 4 of the main article and hence are related.

#### A. Bound states and virtual bound states in square well potential

The notion of a virtual bound state can be most easily illustrated for the case of the square well attractive potential  $V(r) = -V_0\theta(R - r)$  between two particles. The scattering phase shift for partial wave  $l = 0$  is obtained by matching the values and derivatives of the wave functions inside  $u(r) = A \sin(qr)$  and outside  $u(r) = B \sin(pr + \delta)$  the potential at  $r = R$ , rendering  $\delta_0 = \arctan[\tan(qR)\frac{q}{p}] - pR$ . Here  $p = (2m_r W)^{1/2}$ ,  $q = (2m_r[W + V_0])^{1/2}$ ,  $m_r$  is the reduced mass, and  $W$  is the non-relativistic energy. Defining the scattering amplitude  $t$  in the non-relativistic theory as  $S = e^{2i\delta_0} = 1 + 2ipt$ , one can extract  $t$  and determine  $W$  and  $p$  where  $t$  has a pole.

The pole positions and the corresponding wave functions are sketched for several values of the attraction  $V_0$  in Fig. 5 (top row). The poles appear at  $W < 0$  and therefore at imaginary momenta  $p = \pm i|p_B|$ . The bound state is defined as a state with pole at  $p = +i|p_B|$  when the wave function falls exponentially  $e^{ipr} = e^{-|p_B|r}$ , and it is present for large attraction  $V_0$ . As  $V_0$  is decreased, the binding energy of the bound state decreases. As  $V_0$  is reduced further, the bound state turns to virtual bound state, which is defined as a state with a pole at  $p = -i|p_B|$ . Its wave function exponentially increases  $e^{ipr} = e^{|p_B|r}$  therefore it is not a normalizable quantum mechanical state. Such a state is understood to be a result of weakly attractive potential between the scattering particles, where the interaction is not attractive enough to form a bound state. However, the presence of its pole closely below threshold still significantly enhances the cross-section and rate  $N \propto p|t|^2$  at energies above threshold, as shown in Fig. 5 (bottom row). Analogous behavior is observed for other shapes of attractive potential, as demonstrated for the attractive Gaussian potential in video [41].

An example of a virtual bound state features in  $pp$ ,  $pn$  and  $nn$  scattering in the channel  $^1S_0$  with  $I = 1$ , where the measured effective parameters are  $a_0^{pn} \simeq 23.7$  fm and  $r_0^{pn} \simeq 2.7$  fm [39, 40]. This renders a virtual bound state about 66 keV below threshold and a significant peak in cross section above it.

The dependence of observables for decreasing attraction  $V_0$  is shown in Fig. 5 for fixed  $m_r$  and  $R$ . Similar behavior is observed when  $m_r$  is decreased or  $R$  is decreased (while keeping the other two parameters fixed).

#### B. Dependence of $T_{cc}$ binding energy on $m_{u/d}$ or $m_c$

In this section we provide some simple quantum mechanical arguments that the pole position of  $DD^*$  scatter-

$m_c$	ID	$l$	$\Lambda( \vec{P} ^2)$	$E^{lat}$ info $N_L = (24, 32)$	$\chi^2/\text{dof}$	$\{a\}$	$\{a\}$ Covariance	$\delta m_{T_{cc}}$ [MeV]	$\bar{X}_A$
$m_c^{(h)}$	1	0	$T_1^+(0)$ $A_2(1)$	(1000, 1100) (10, 10)	1.3/3	$a_0^{(1)} = 1.13^{(+0.37)}_{(-0.34)} \text{ fm}$ $r_0^{(1)} = 0.94^{(+0.19)}_{(-0.20)} \text{ fm}$	1.00 0.06 1.00	$-8.9^{(+3.2)}_{(-7.0)}$	0.61(7)
	2	0,1	$T_1^+(0)$ $A_2(1)$ $A_1^-(0)$	(1000, 1100) (11, 11) (1, 1)	3.7/5	$a_0^{(1)} = 1.04(0.29) \text{ fm}$ $r_0^{(1)} = 0.96^{(+0.18)}_{(-0.20)} \text{ fm}$ $a_1^{(0)} = 0.076^{(+0.008)}_{(-0.009)} \text{ fm}^3$ $r_1^{(0)} = 6.9(2.1) \text{ fm}^{-1}$	1.00 0.13 -0.28 -0.18 1.00 0.02 0.02 1.00 0.65 1.00	$-9.9^{(+3.6)}_{(-7.2)}$	0.59(6)
$m_c^{(l)}$	3	0	$T_1^+(0)$ $A_2(1)$	(1000, 1100) (10, 10)	1.4/3	$a_0^{(1)} = 0.94(0.25) \text{ fm}$ $r_0^{(1)} = 0.96^{(+0.18)}_{(-0.20)} \text{ fm}$	1.00 0.06 1.00	$-12.9^{(+4.1)}_{(-8.2)}$	0.57(6)
	4	0,1	$T_1^+(0)$ $A_2(1)$ $A_1^-(0)$	(1000, 1100) (11, 11) (1, 1)	3.6/5	$a_0^{(1)} = 0.86(0.22) \text{ fm}$ $r_0^{(1)} = 0.92^{(+0.17)}_{(-0.19)} \text{ fm}$ $a_1^{(0)} = 0.117^{(+0.013)}_{(-0.014)} \text{ fm}^3$ $r_1^{(0)} = 8.6^{(+1.5)}_{(-1.1)} \text{ fm}^{-1}$	1.00 0.12 0.09 -0.11 1.00 -0.03 0.04 1.00 -0.95 1.00	$-15.0^{(+4.6)}_{(-9.3)}$	0.56(5)

TABLE I. Details and results of the scattering analysis: the partial waves considered, the finite-volume energies included, the quality, the best fit values and the covariances for the resulting parameters of various fits. In the last two columns, we also present the binding energy and a compositeness measure, as defined in Ref. [39], of the  $l = 0$  virtual bound state.

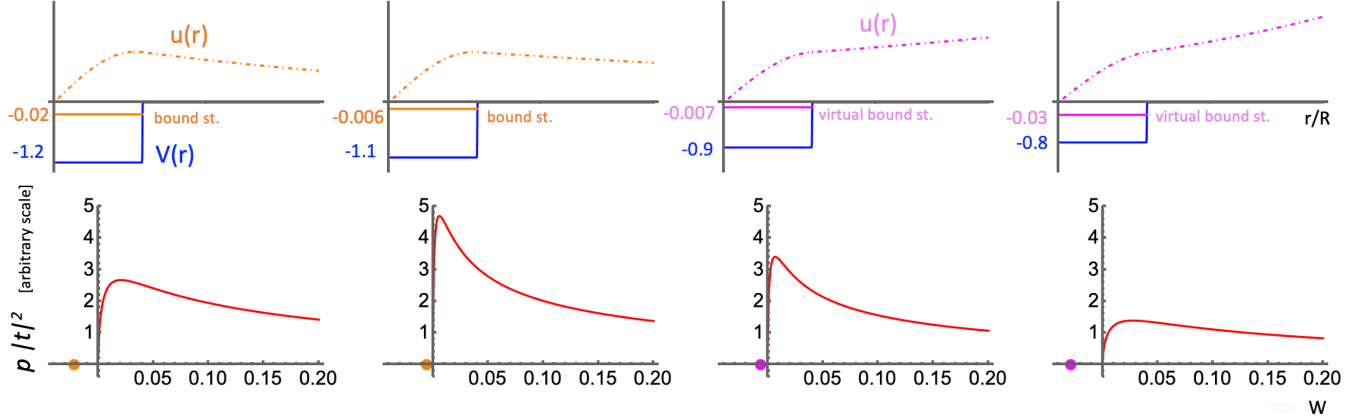


FIG. 5. Dependence of various observables related to the scattering in the square-well potential as the attraction potential  $V_0$  (blue) is decreased, while  $R = 1$  and  $m_r = \pi^2/8$  are fixed. The bound state (orange) becomes a virtual bound state (magenta) at  $V_0 = 1$ . Top: Energy  $W < 0$  where the scattering amplitude has a bound state pole (solid orange) or a virtual bound state pole (solid magenta), as well as the corresponding wave functions at these energies (dot-dashed). Bottom: The scattering rates  $N \propto p|t|^2$  above threshold (red) are enhanced due to the poles closely below threshold (orange/magenta circles).

ing in partial wave  $l = 0$  roughly varies with changing  $m_{u/d}$  or  $m_c$  as sketched in Fig. 4 of the main article. We consider a pole related to the state dominated by a *molecular Fock component*. The pole positions found by LHCb and by our lattice study at two charm quark masses are in line with these arguments. However, further lattice studies at various quark masses are needed to establish these arguments empirically.

We investigate position of the pole for purely attractive potential  $V(r) = -V_0 f(r)$  between  $D$  and  $D^*$  with  $V_0 > 0$ . We explored various shapes, for example the Yukawa  $f(r) = e^{-r/R}/r$ , exponential  $f(r) = e^{-r/R}$ , square-well  $f(r) = \theta(R - r)$ . For a given potential, we numerically determined the phase-shift  $\delta_0$ , the scattering amplitude

and the energy, where scattering amplitude has a pole. We focused on the potentials where the pole is close to the threshold. The qualitative behavior for all potentials is analogous to the one derived analytically in the previous subsection for the square-well potential, as also shown in the video [41]. A typical dependence of the pole position on varying one of the parameters in potential ( $V_0$ ,  $R$ ) or the reduced mass  $m_r$  is shown in Fig. 6. The bound state is present for large attraction  $V_0$ . As  $V_0$  is decreased, the binding energy of the bound state decreases, at critical  $V_0$  it turns to a virtual bound state and then the pole moves further below threshold. Analogous behavior is observed when  $m_r$  or  $R$  are decreased. Note that the bound state does not turn to a resonance for a purely

attractive potential since there is no barrier to keep the resonance metastable.

Let us now consider how the quark masses affect the values of  $V_0$ ,  $R$ ,  $m_r$  and thereby the pole positions. As  $m_{u/d}$  increases, the mass of the exchanged light mesons  $M$  also increases and the range of the potential  $R \simeq 1/M$  decreases, which renders the dependence on  $m_{u/d}$  sketched in Fig. 4 of the main article. Here we assumed that the dependence of the reduced mass on  $m_{u/d}$  is negligible.

The decrease of  $m_c$  will decrease the reduced mass  $m_r$  of the  $DD^*$  system, while the potential will not change drastically due to the heavy quark flavor symmetry. The bound state becomes less and less bound with decreasing  $m_c$  and eventually turns to a virtual bound state. As  $m_c$  is decreased further, the virtual bound state pole moves further below threshold and the influence of this pole on the scattering above threshold is diminished.

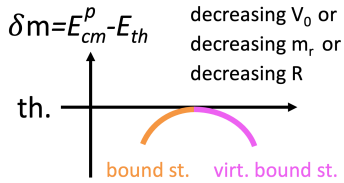


FIG. 6. Sketch of the binding energy for the (virtual) bound state dominated by the molecular component in quantum mechanics with a purely attractive potential:  $V_0$  is its overall size,  $R$  is the range and  $m_r$  is the reduced mass.

Now let us turn to quark mass dependence of the bound state dominated by the *diquark antidiquark Fock component*  $[QQ][\bar{u}\bar{d}]$ . The attractive colour Coulomb potential between two heavy quarks in diquark  $[QQ]$  is flavor blind, while the kinetic energy increases with decreasing  $m_Q$ . This implies that the binding energy decreases with decreasing  $m_Q$ . The attraction within the good light diquark  $[ud]$  becomes less significant as  $m_{u/d}$  increases [24], which implies that the binding energy will decrease. This is in line with the sketch for the bound state behavior in Fig. 4 of the main article, which is supported by the phenomenological studies [9, 11] and lattice studies of  $bb\bar{u}\bar{d}$  [16–21, 23]. However, it is not known from lattice simulations yet what is the fate of a pole when a diquark antidiquark state is on the verge of binding and whether it would turn to a resonance or virtual state. The analytical considerations of compositeness in Ref. [39] suggest that compact states exist as bound states or resonances.